PERGAMON

Continental Shelf Research 21 (2001) 1191–1218

CONTINENTAL SHELF RESEARCH

www.elsevier.com/locate/csr

Variability in coastal zone color scanner (CZCS) Chlorophyll imagery of ocean margin waters off the US East Coast

J.A. Yoder[a,*], J.E. O'Reilly[b], A.H. Barnard[a,1], T.S. Moore[a,2], C.M. Ruhsam[a]

[a] *Graduate School of Oceanography, University of Rhode Island, Narragansett, RI 02882, USA*
[b] *NOAA/National Marine Fisheries Service, Northeast Fisheries Science Center, Narrangansett, RI 02882, USA*

Received 15 December 1999; accepted 8 June 2000

Abstract

The purpose of our study was to use the 7.5-year coastal zone color scanner (CZCS) image time series (Oct. 1978 to July, 1986) to study general patterns in near-surface phytoplankton chlorophyll concentrations in ocean margin waters off the US East Coast. We defined 21 relatively large study areas ($>100\,km^2$) within the MAB and SAB to set boundaries for averaging and subsequent analyses. Our objective was to partition the observed CZCS-derived chlorophyll concentration (CSAT, $mg\,m^{-3}$) variability of these 21 study areas within three general categories based on time scale: daily (i.e. day–week), seasonal and interannual. An additional objective was to determine relations between the temporal patterns in the 21 study areas. All available CZCS imagery (more than 3500 scenes of Level 1 imagery, i.e. top-of-the-atmosphere radiance in satellite swath coordinates) covering some or all of our area of interest (northwest Atlantic off the US East Coast) were obtained at full resolution, processed to Level 2 (water-leaving radiance, chlorophyll concentration and other derived products in satellite swath coordinates) and mapped to two different study regions located off the southeast and northeast coasts of the US. Satellite-derived estimates of near-surface chlorophyll concentrations (CSAT) were extracted on a pixel-by-pixel basis from each of the 21 study areas (chosen based on oceanographic criteria) from each of the daily composite CSAT images. For each image and when satellite coverage permitted, CSAT values were averaged to yield a time series of daily mean values for each of the 21 study areas. We used three basic approaches to quantify temporal and spatial patterns in the 21 time series: (1) multiple linear correlation, (2) structure functions (semi-variance calculations) and (3) empirical orthogonal functions (EOF). Our results show:

(1) a simple annual CSAT cycle common to all ocean margin waters along the entire US East Coast, consisting of a broad peak in CSAT concentration during winter and minimum concentrations during the summer;

*Corresponding author. Fax: 1-401-874-6728.
E-mail address: jyoder@gso.uri.edu (J.A. Yoder).
[1] Now located at Bigelow Laboratory for Ocean Sciences, P.O. Box 475, West Boothbay Harbor, ME 04575, USA.
[2] Now located at Ocean Process Analysis Lab, Morse Lab, University of New Hampshire, Durham, NH 03824, USA.

PII: S0278-4343(01)00009-7

(2) relatively subtle across- and along-shelf changes to the timing and relative magnitude of the winter CSAT maxima and summer minima, as well as the presence of secondary seasonal peaks in some regions;
(3) high variability at time scales of days to weeks superimposed on the seasonal pattern;
(4) high spatial coherence of the seasonal component between all 21 study areas;
(5) high coherence of the days-to-weeks component between adjacent study areas, but generally low or no coherence for study areas not adjacent or near each other; and
(6) detectable, but low interannual variability.

Keywords: Satellite sensing; Phytoplankton; Continental shelves; Algal blooms; CZCS; Ocean color; Ocean variability

1. Introduction

Our study focuses on continental shelf and slope waters off the US East Coast from just south of Cape Canaveral, Florida to Georges Bank (Fig. 1). Cape Hatteras, North Carolina separates this region into two distinct regimes: the South Atlantic Bight (SAB) and the Mid Atlantic Bight (MAB) (Fig. 1). Both regimes have a relatively broad shelf with the 200-m isobath located more than 100-km from the coast in the central portion of each bight. The cyclonic side of the Gulf Stream is generally near the 200-m isobath in the SAB (Menzel et al., 1993), whereas the Gulf Stream front is much farther offshore north of Cape Hatteras (Beardsley et al., 1976) (Fig. 1). As a

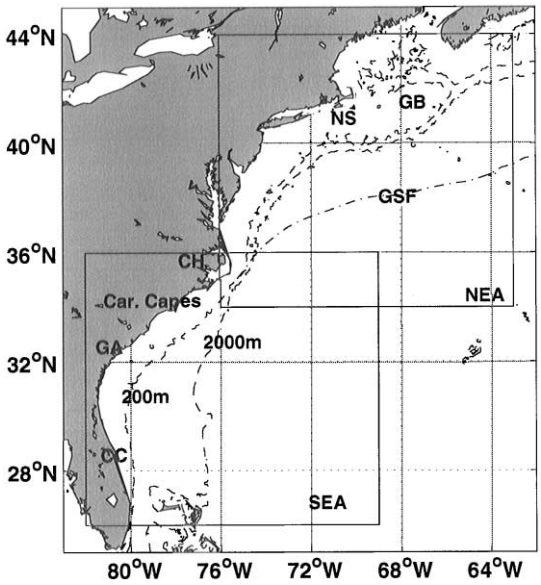

Fig. 1. Chart of the northwest Atlantic off the US East Coast. Two large boxes show NEA and SEA regions used for mapping CZCS imagery. Letters indicate locations and geographic regions referred to in the text where (starting at lower left): CC—Cape Canaveral; GA—State of Georgia; Car. Capes—Carolina Capes; CH—Cape Hatteras; NS—Nantucket Shoals; and GB—Georges Bank. Two isobaths (200 and 2000 m) are shown as is the mean position of the Gulf Stream front (GSF) north of Cape Hatteras.

result, a slope water mass (slope sea) lies between the shelfbreak (ca. 200 m isobath) and the Gulf Stream front in the MAB (Csanady, 1990) but is absent in the SAB (Fig. 1).

In situ and satellite studies identified many processes affecting spatial and temporal variability in phytoplankton biomass and productivity in the SAB and MAB. Seaward of the 20-m isobath in the SAB, upwelling and intrusion of nutrient-rich waters associated with frontal eddies and meanders of the Gulf Stream front stimulate surface and subsurface phytoplankton blooms (Verity et al., 1993; Pribble et al., 1994). The frontal region itself often has enhanced phytoplankton chlorophyll concentrations caused by mixing related to wind and Gulf Stream interactions (Ryan and Yoder, 1996). Seasonal phytoplankton blooms, including the spring bloom, are important in shelf and slope waters of the MAB (Riley, 1946, 1947; Ryther and Yentsch, 1958) and have a strong signal in ocean color imagery (Brown et al., 1985). Phytoplankton distribution patterns in slope waters are also influenced by Gulf Stream rings (Garcia-Moliner and Yoder, 1994), and mixing associated with frontal dynamics leads to enhanced phytoplankton biomass concentrations and productivity in the shelf-slope frontal region compared to adjacent waters (Marra et al., 1990; Ryan et al., 1999a, b). MAB wind events throughout the year change the distribution of pigment in the water column and lead to higher phytoplankton growth and productivity in response to increased nutrient flux (Walsh et al., 1978, 1987). These and other processes are known to affect phytoplankton biomass variability in the SAB and MAB at time scales ranging from days to season and possibly at longer time scales as well. Furthermore, dominant processes affecting phytoplankton biomass and productivity change along and across the shelf and slope, so that temporal patterns in phytoplankton biomass are not always spatially coherent within the East Coast shelf/slope ecosystem.

The purpose of our study is to use the 7.5-year coastal zonc color scanner (CZCS) image time series (Oct. 1978 to July, 1986) to study general patterns in near-surface phytoplankton chlorophyll concentrations. We define 21 relatively large study areas within the MAB and SAB to set boundaries for averaging and subsequent analyses. Our objective is to partition the observed CZCS-derived chlorophyll concentration (CSAT, $mg\,m^{-3}$) variability of these 21 study areas within three general categories based on temporal scale: daily (i.e. day–week), seasonal and interannual. An additional objective is to determine the spatial coherence of the temporal patterns throughout the 21 study areas.

2. Methods

All available CZCS imagery (more than 3500 scenes of Level 1 imagery i.e. top-of-the-atmosphere radiance in satellite swath coordinates) covering some or all of our area of interest (northwest Atlantic off the US East Coast, Fig. 1) was obtained at full resolution (1×1 km nominal pixel resolution) from NASA-Goddard Space Flight Center. Using the University of Miami's DSP software, Level 1 imagery was processed to Level 2 (water-leaving radiance, chlorophyll concentration and other derived products in satellite swath coordinates) using Gordon's multiple scattering atmospheric correction algorithm with revised calibration coefficients (Gordon et al., 1983; Evans and Gordon, 1994). Based on our evaluation and analysis of East Coast imagery, we used mean East Coast epsilon values (ECOAST values, see Table 2a in Bisagni et al., 1997) during the processing to remove the aerosol contribution from

top-of-the-atmosphere radiance. We used a 3-band bio-optical algorithm (Clark, 1981) to convert water-leaving radiance at 443, 520 and 550 nm to estimates of chlorophyll concentration, which is generally interpreted as the sum of chlorophyll a + pheopigments (Clark, 1981); hereinafter referred to as CSAT ($mg\,m^{-3}$). The 3-band algorithm generally yields a log-normal CSAT distribution in continental shelf and slope waters, rather than a bi-modal distribution (Denman and Abbott, 1988) typifying high-chlorophyll imagery processed with the NASA standard CZCS bio-optical algorithm. The latter switches between two, 2-band ratio algorithms depending upon the chlorophyll concentration (Feldman et al., 1989).

Level 2 CSAT standard scenes (2-min of observations) were mapped to two, 512×512 pixel equirectangular projections: off the southeastern and northeastern US coast (SEA and NEA, respectively) (Fig. 1). Daily composites were formed when more than one scene was available for a single day. There were 1121 and 1114 daily composite images, with at least some cloud-free pixels, covering SEA and NEA projections, respectively. After mapping, images had a nominal pixel resolution of ca 2×2 km. Final navigation of each image was done by hand using the coastline for a reference. Cloud masking (i.e. assigning cloud pixels a numerical value indicating that these pixels are to be excluded from all subsequent calculations) is part of the standard DSP processing of CZCS imagery. However, some cloud-induced artifacts (e.g. "ringing") pass through the standard cloud masking calculations, particularly down scan (more or less to the East) from clouds. To further eliminate cloud artifacts and similar artifacts down scan from land, we masked an additional 10 pixels (ca. 20-km) down scan and 1 pixel up scan from all cloud and land pixels identified by the standard algorithm. This is a conservative approach in that it also masks some valid data. However, the remaining unmasked pixels are substantially free of cloud artifacts.

Fig. 2 shows the 21 study areas from which we extracted CSAT concentrations on a pixel-by-pixel basis from all of the CZCS daily composites in the time series. Areas 1–10 are in the SEA, and we defined the boundaries of these 10 areas based on previous criteria used to subdivide this region for satellite and other studies (Yoder, 1985; McClain et al., 1988; Lee et al., 1991; Menzel et al., 1993; Ryan and Yoder, 1996). The inner boundary of areas 1–4 is the 20-m isobath generally considered to be the outer boundary of the SAB (SEA) inner shelf. The outer boundary of these 4 areas and the inner boundary of regions 5–8 is the 40-m isobath, whereas the outer boundary of areas 5–8 is the 200-m isobath. Thus, areas 1–4 cover the middle shelf and areas 5–8 are the outer shelf, using terminology in the references cited above. In the along-shelf direction, we separated the SEA into three general regions again based on results of prior studies (see above references). Areas 1 and 5 are off the North Florida coast, areas 2, 3, 6 and 7 are in the Georgia Bight and areas 4 and 8 are in the Carolina Capes regions (McClain et al., 1988). Area 9 is in the Gulf Stream, and area 10 is seaward of the Gulf Stream over the Blake Plateau where water depths exceed 500 m. Area 10 was used to check for long-term change (drift) in mean CSAT concentration within predominantly blue oceanic waters during the 7.5 year time series.

Isobath ranges were also used as a key criteria for choosing NEA (MAB) study areas. Areas 11 and 12 are between the 40 and 200-m isobaths on the narrow shelf just north of Cape Hatteras. Areas 13–15 cover the middle shelf between the 25 and 60-m isobaths, and areas 17–19 cover the outer shelf between the 60 and 200-m isobath. Areas 20 and 21 cover slope waters between the 200-m isobath and the mean position of the Gulf Stream front as determined from climatological SST observations (Cornillon, 1992). Area 16 (Georges Bank) is enclosed by the 80-m isobath. The NEA was subdivided in the along-shelf direction based on the location of MARMAP transects

Fig. 2. Study areas in ocean margin waters off the US East Coast (see Fig. 1 for geographic reference). (A). Middle shelf areas 1–4 are bounded by the 20 and 40 m isobaths; outer shelf areas 5–8 by the 40 and 200 m isobaths; area 9 is the Gulf Stream and area 10 is in oceanic waters of the Blake Plateau. (B) Middle shelf areas 11 and 12 are bounded by 20 and 40 m isobaths and middle shelf areas 13, 14 and 15 by the 25 and 60 m isobaths; area 16 is enclosed by the 80 m isobath; outer shelf areas 17, 18 and 19 are bounded by the 60 and 200 m isobaths; and slope water areas 20 and 21 by the 200 m and the mean position of the cyclonic side of the Gulf Stream.

A-E (O'Reilly and Zetlin, 1998). MARMAP was an extensive, NOAA-National Marine Fisheries Service (NMFS) multiyear study of the MAB ecosystem. MARMAP investigators measured chlorophyll *a* concentrations from 78 oceanographic cruises between 1977 and 1988 (O'Reily and Zetlin, 1988), i.e. overlapping the CZCS observation period.

To build spatially averaged (geometric mean owing to the log-normal distribution) time series, CSAT values were extracted on a pixel-by-pixel basis from each of the 21 study areas from each of the daily composite CSAT images. In principle, the CZCS should have covered a given location off the US East Coast every day or two, but owing to cloud cover and mission operations (i.e. the CZCS instrument was not always operating during the mission), the number of daily images covering some or all of each study area was substantially less than the total number of days during the 7.5 years of the time series. Furthermore, different study areas were often covered on different days, and at times, none or only a very small percentage of the pixels within a given study area were unmasked owing to high cloud cover. To choose an appropriate pixel coverage criteria for

including a daily, spatially-averaged CSAT concentration in our time series, we compared time series using daily spatial averages based on at least 5%, 25% and 50% of unmasked pixels. As for other investigations (e.g. McClain et al., 1988), we found that the time series patterns and overall daily mean CSAT concentrations were very similar (overall means within a few percent) for the two series based on at least 25% and 50% unmasked pixels. The number of days in the time series (i.e. number of observations) increased by 1.35X when using 25% versus 50% unmasked pixel criteria. For these reasons, we built our daily time series for each of the 21 study areas by calculating the geometric mean of CSAT pixel values extracted from each study area for which 25% or more of that area's pixels were unmasked. These time series were used for all further calculations, and Table 1 shows the overall mean and number of observations for each daily time series.

Routines written in *Matlab* (The Mathworks, Inc.) were used for the analyses of the 21 time series extracted from the CZCS satellite images. We used three basic approaches to quantify temporal and spatial patterns in the 21 time series: (1) multiple linear correlation, (2) structure functions (semi-variance calculations) (e.g. Yoder et al., 1987), and (3) empirical orthogonal functions (EOF).

Multiple linear correlation was performed on different CSAT subsets of the 21 time series (e.g. all 11 time series from the NEA region) after first finding common sampling days. In other words, daily CSAT time series from each of the study areas do not always have observations from the same day (owing to differences in image coverage). Thus, the multiple linear correlation was performed on daily CSAT values that were common to all of the members of each subset analyzed.

Structure functions, i.e. semi-variance (SV) versus lag time (h), for lag times ranging from 1 to 250 days were calculated for each time series (2745 days long) according to Eq. (1) (Yoder et al., 1987).

$$\mathrm{SV}_{(\mathrm{lag}=h)} = 1/2N_h \sum_{x=1}^{x=2745} (G_x - G_{(x+h)})\hat{}\,2, \tag{1}$$

where SV is the semi-variance, h the lag time (from 1 to 250 days), N_h the number of observations for each lag, h, and G_x the sample value (CSAT) at time $= x$, $G_{(x+h)}$ = sample value at time $= x + h$, and $x = 2745$ days is the length of the time series.

Structure functions (semi-variograms), i.e. graphs of SV versus lag time for each lag time from 1 to 250 days, were generally quite noisy. To reduce noise and highlight dominant temporal scales, semi-variance was smoothed by 4X decimation, and then a third degree polynomial was fit to the filtered semi-variance as a function of lag time. The results were graphically interpreted using consistent criteria (Yoder et al., 1987) to find either peaks or asymptotes of the semi-variograms.

EOF analyses require time series of evenly spaced data without significant gaps, and our 7.5-year time series of daily CSAT time series had far too many missing values for this technique. We thus created a second time series for each of the 21 study areas based on 45-day temporal bins. The 45-day averaging period was the shortest interval possible with at least one data point in 90% of the bins for each time series. We also wanted each year to have an equal number of bins (8×45 days) and with the first bin of every "year" centered on the winter solstice starting with bin number 1 centered on 22 December, 1978. The other seven bins for each year of the 7.5-year

CZCS time series (total = 60 bins) were centered on 4 February, 22 March, 6 May, 22 June (summer solstice), 15 August, 20 September and 5 November. To keep every eighth bin centered on the winter solstice, bins 1, 9, 17, 25, 33, 41, 49 and 57 (i.e. the final bin of each year) were 5 (or 6) days longer than the other bins. Owing to clouds and other factors, bins differed in the number of daily CSAT observations making up the average bin value, and in some cases, a single CSAT value represented the temporal bin. When more than one daily CSAT value was available for a 45-day binning period, the geometric mean was used to represent the bin (as is appropriate for log-normally distributed data).

EOF calculations using the covariance matrix technique were performed on the 45-day binned time series for areas 1–21 using software provided by A. Barnard and T. King. Most of the time series had some missing values, so an objective estimate of the amplitude was calculated by estimating the projection of the EOF onto the non-missing spatial locations. EOFs for the 11 NEA regions and for SEA regions 1–8 were calculated separately, as the NEA and SEA are distinct oceanographic regimes. We calculated EOFs using several different data pretreatment approaches, including no pretreatment. For the results presented here, which are representative of the different approaches we tried, the data were pretreated in two different ways. For the first, which emphasizes temporal trends, the EOF calculations were done on the log of the time series and for each time series, the overall mean of the 60 bins was subtracted from each element. For the second, which emphasizes changes to the spatial pattern with time, we computed standardized EOFs by first subtracting the spatial mean for each time interval from each time series element and then dividing by the standard deviation, before computing eigenvectors and amplitude time series (Fuentes-Yaco et al., 1997).

3. Results

3.1. Simple statistics

Figs. 3 and 4 are monthly mean composite CSAT images for the SEA and NEA regions consisting of all of the available data from the 7.5-year CZCS time series. The composite monthly images for the SEA show very persistent spatial patterns dominated by the across-shelf gradient and with little apparent along-shelf variability (Fig. 3). The band of relatively high CSAT, i.e. boundary between green and blue ($>0.5\,\mathrm{mg\,m^{-3}}$), extends farther offshore in winter than during the summer (compare December through February images with June through August images). Monthly mean images for the NEA (Fig. 4) show more spatial variability than for the SEA, particularly on Nantucket Shoals (immediately south of Cape Cod) and Georges Bank (offshore and east of Cape Cod). The effects of Gulf Stream rings (particularly ring 82-B which was captured in many individual images in 1982 (e.g. Garcia-Moliner and Yoder, 1994) are clearly visible in the April composite (center left of the image).

The monthly composite images in Figs. 3 and 4 hide a greatly deal of temporal and spatial variability. Table 1 shows simple statistics for the 21 time series. For each time series, the magnitudes of the standard deviation and arithmetic mean are of comparable magnitude as the arithmetic mean, including high temporal variability during the time series. Not shown are the standard deviations associated with spatial averaging of pixel values extracted from the

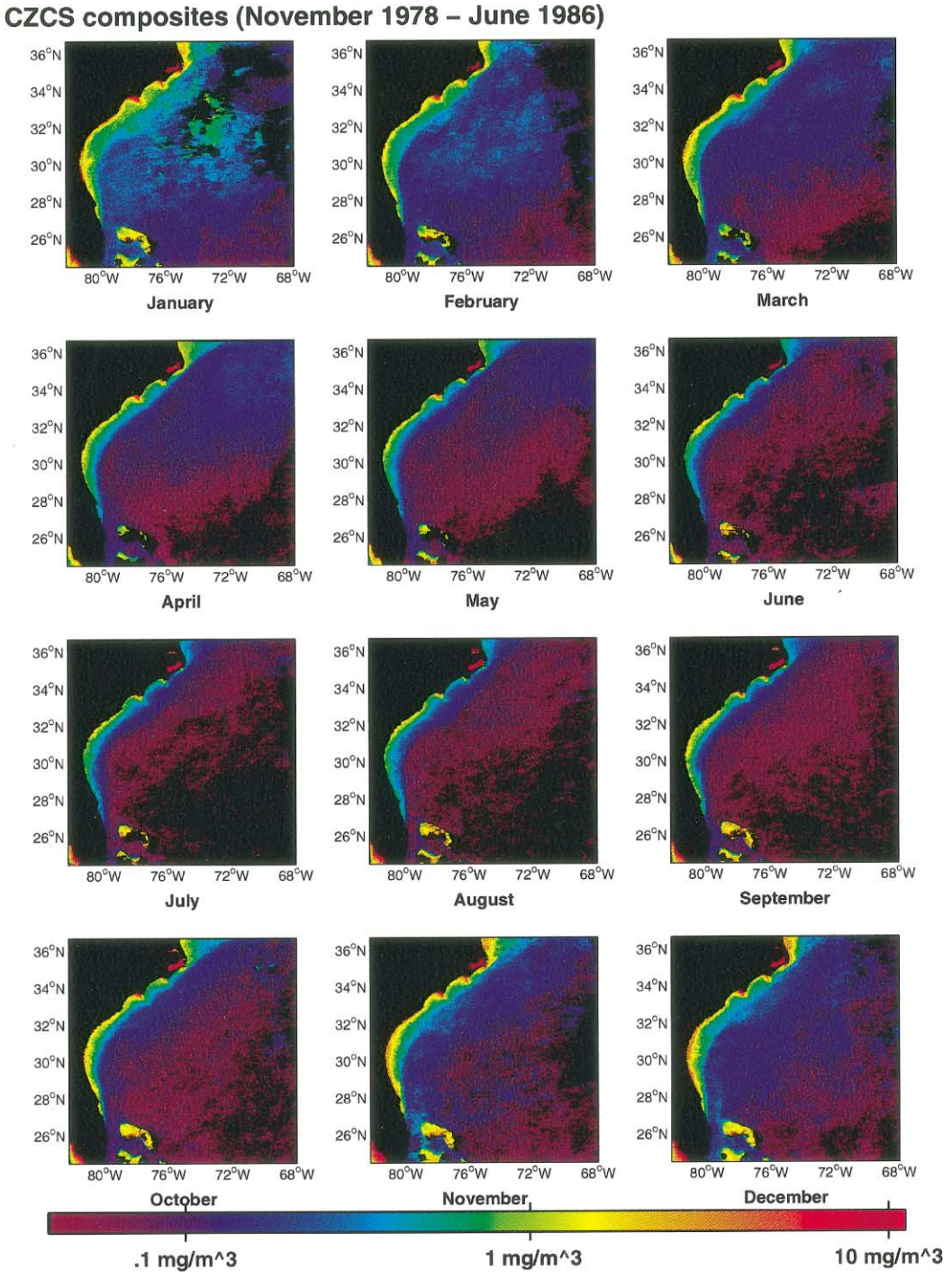

Fig. 3. Monthly composite CSAT images for the SEA study area. Color bar at the bottom of the figure indicates CSAT concentration ($mg\,m^{-3}$) range and black pixels indicate no valid data. Apparently high CSAT concentrations (>0.50) surrounding the Bahama banks (off Florida) are an artifact owing to bottom reflection and shallow, clear water.

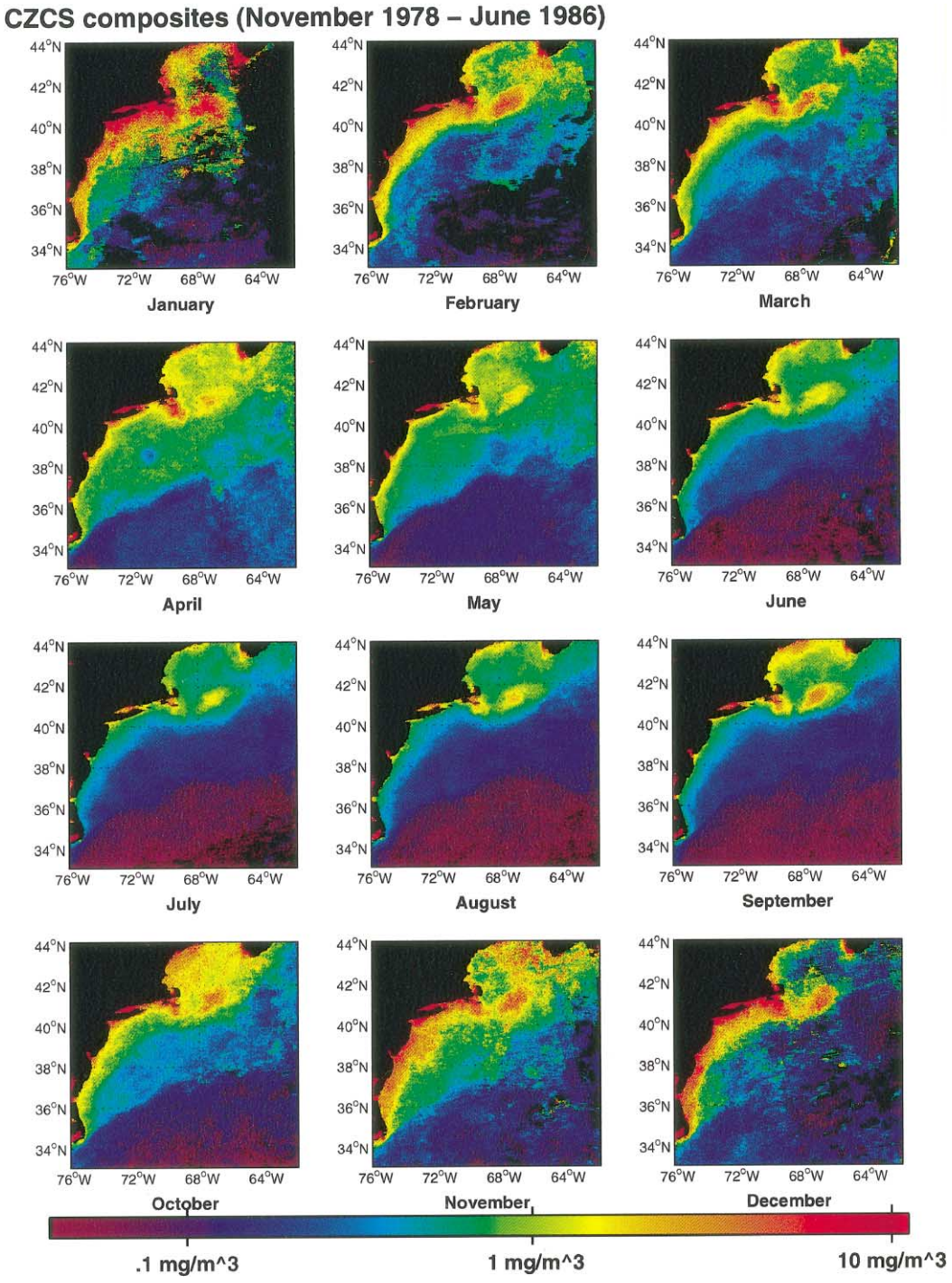

Fig. 4. Monthly composite CSAT images for the NEA study area.

Table 1
Simple statistics for the 21 time series of daily average CSAT concentration (>25% pixel coverage) from study areas illustrated in Fig. 2, as well as statistics for NEA areas 11–21 and SEA areas 1–8. *N* is the number of days having a valid (25% pixel coverage) CSAT observation during the 7.5-year (2745 day) time series

Area	*N*	Arith. mean	S.D.	Geom. mean
1	231	1.17	1.45	0.80
2	252	0.94	0.98	0.70
3	446	0.75	0.69	0.59
4	467	0.65	0.50	0.53
5	205	0.39	0.30	0.32
6	244	0.42	0.45	0.31
7	89	0.41	0.41	0.32
8	370	0.31	0.25	0.25
9	194	0.13	0.11	0.11
10	189	0.10	0.07	0.09
SEA (1–8)	2604	0.62	0.73	0.44
11	251	0.88	0.95	0.62
12	281	0.96	1.22	0.66
13	421	1.36	1.46	0.94
14	460	1.77	1.86	1.17
15	414	2.16	2.13	1.48
16	309	1.60	1.40	1.21
17	422	0.85	1.01	0.59
18	409	1.02	1.20	0.69
19	384	0.97	1.19	0.65
20	369	0.57	0.60	0.41
21	344	0.58	0.72	0.39
NEA	4064	1.19	1.44	0.75

daily composite images (which yields the individual CSAT values comprising the time series), and which are also of equivalent magnitude to the spatial mean for each member of the time series. This within study area spatial variability (covering scales in the 1 to <100 km range) is not considered further in this manuscript (but see Yoder et al., 1987). Fig. 5 shows the frequency distributions (Log 10 CSAT) for all the NEA study areas and SEA study areas 1–8 (shelf/slope water study areas) indicating that a log-normal distribution is a reasonable approximation for the distribution of these data.

3.2. Comparison with in situ data

Fig. 6 shows MARMAP in situ near-surface chlorophyll *a* + pheopigments and CSAT concentrations ($mg\,m^{-3}$) versus yearday for NEA study areas representing middle shelf (areas 13, 14), outer shelf (areas 17, 18) and slope waters (areas 20 and 21). Each CSAT point is an average for that portion of a daily image covering the study area, and the in situ concentrations

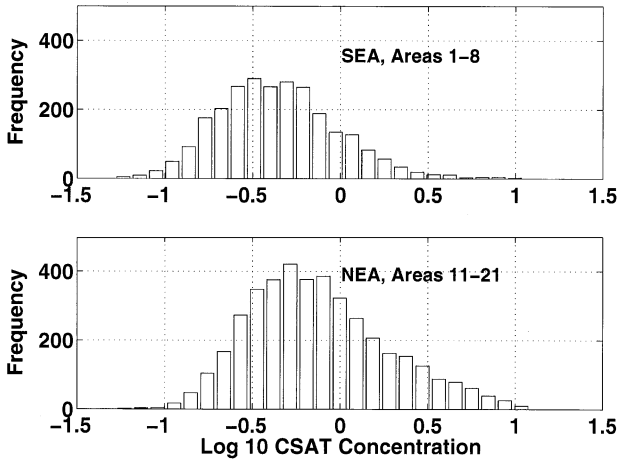

Fig. 5. Frequency distribution of Log_{10}CSAT concentrations (mg m^{-3}) comprising time series for SEA study areas 1–8 (n =2604 daily mean values) and NEA study areas 11–21 (n =4064 daily mean values).

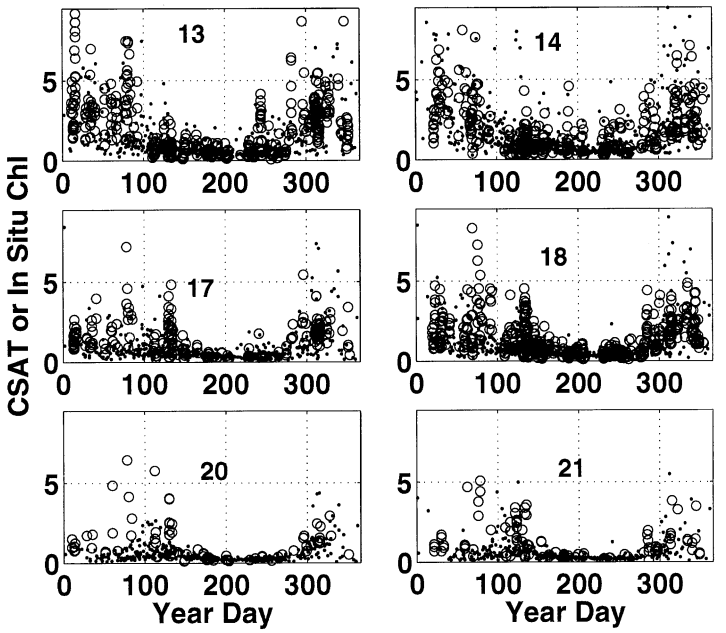

Fig. 6. MARMAP in situ near-surface chlorophyll a+pheopigments (open circles) and CSAT concentrations (dots) (mg m^{-3}) versus yearday for representative NEA study areas (13 and 14—middle shelf; 17 and 18—outer shelf; and 20 and 21—slope). In situ concentrations are single station values, whereas CSAT concentrations are the daily mean for that portion of the image covering each study area.

are single station values. Previous analyses (using space/time matchups between CSAT and in situ data) showed that CSAT values based on the Clark (1981) algorithm underestimates in situ chlorophyll a+pheopigment concentrations in the MAB (J.E. O'Reilly, personal communication). This is also characteristic of the results depicted in Fig. 6, as geometric mean CSAT (0.67,

$n = 2425$) for areas 13, 14, 17, 18, 20 and 21 was 59% of the geometric mean of the in situ data (1.14, $n = 1705$). Of primary importance in this study, however, is that Fig. 6 shows no systematic difference between the mean seasonal distribution of CSAT and MARMAP data. Both show that maximum concentrations occur during fall–winter (i.e. after year day 300 and before year day 100), particularly in middle and outer shelf waters (areas 13, 14, 17 and 18). Slope waters (20 and 21) also have a fall–winter maximum after year day 300, but then show a distinct spring maximum near yearday 100, as previously reported from CSAT imagery (e.g. Brown et al., 1985). It is also obvious from Fig. 6 that there is generally a much wider range in CSAT and MARMAP surface chlorophyll concentrations during fall–winter–spring (yearday > ca. 300 and < 150) than during the summer stratified period of the year (ca. 150 < yearday < ca. 250), when concentrations are generally quite low ($< 0.5\,\mathrm{mg\,m^{-3}}$).

Mean trends in CSAT data are also similar to mean in situ water column chlorophyll (MARMAP averages, O'Reilly and Zetlin, 1998) in the NEA (Fig. 7). This is somewhat surprising in that water column averages also include samples from depths as deep as 75-m, well below the sensing depth of ocean color scanners. Also, the data are not precise matchup data, i.e. the averages are for very general areas (middle shelf, outer shelf, etc.) within a general region (NFA) and during roughly, but not exactly, the same time period (1978–1986). In area 20, CSAT estimates during the summer (water column stratified) are systematically lower than in situ measurements because a pronounced subsurface chlorophyll maximum layer, 20–35 m below surface, contributes to the water column average but has little influence on the upwelling light detected by CZCS (O'Reilly and Zetlin, 1998). The results in Fig. 7 show biggest differences

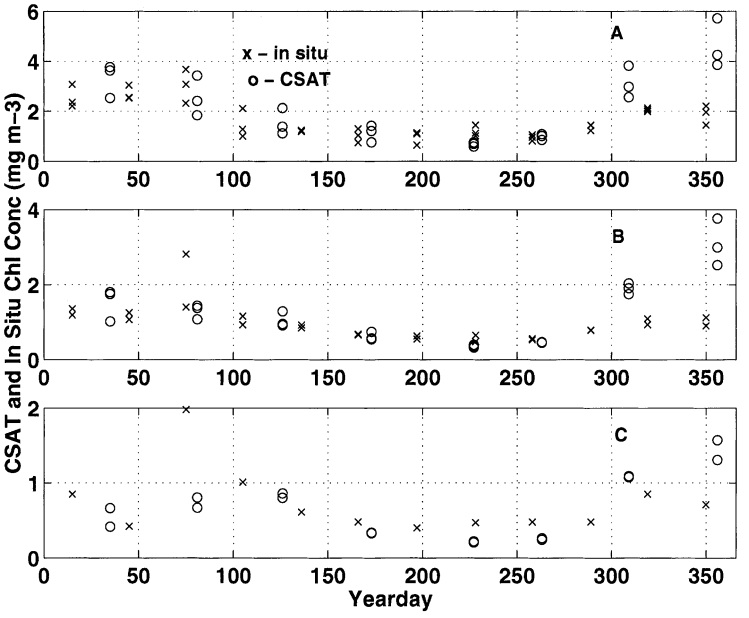

Fig. 7. CSAT and in situ chlorophyll (MARMAP water column averages from Table 3 in O'Reilly and Zetlin, 1998) time series from middle shelf (A), outer shelf (B) and slope waters (C) in the NFA. CSAT values are plotted versus the yearday midpoint of the 8 bins, and in situ values are plotted against the yearday equivalent of the monthly midpoint.

between CSAT and in situ data after yearday 300 indicating that an analysis of seasonal patterns based on CSAT data may overemphasize the importance of the early winter period to the annual mean chlorophyll concentration compared to in situ concentrations. However, both time series in Fig. 7 do show that chlorophyll concentrations begin to increase near yearday 290; and that this winter period of comparatively high chlorophyll is sustained through the remainder of the year and until yearday 150 or so of the following calendar year.

3.3. Variability in the time series extracted from daily composited images

Fig. 8 shows time series examples (areas 2, 6, 13 and 20) from the 21 study areas and illustrate some key features of all the time series. First, a seasonal signal is evident in all years, particularly in the NEA (areas 13 and 20 in Fig. 8), with highest CSAT concentrations during winter and lowest in summer. Higher frequency variability at the days to weeks time scale is also very evident in all years, particularly during the fall–winter–spring period. Finally, temporal gaps are obvious throughout the time series, and the latter characteristic makes the daily time series unsuitable for standard time series statistics (e.g. spectral analysis).

Table 2 shows the results of multiple linear correlation between some of the CSAT time series. Regressions were performed on same-day values (Log_{10} CSAT) within each group shown in Table 2. Subgroups were selected for comparisons in part to keep the number of same-day observations relatively high, as for example, there were only 2 common observations among the

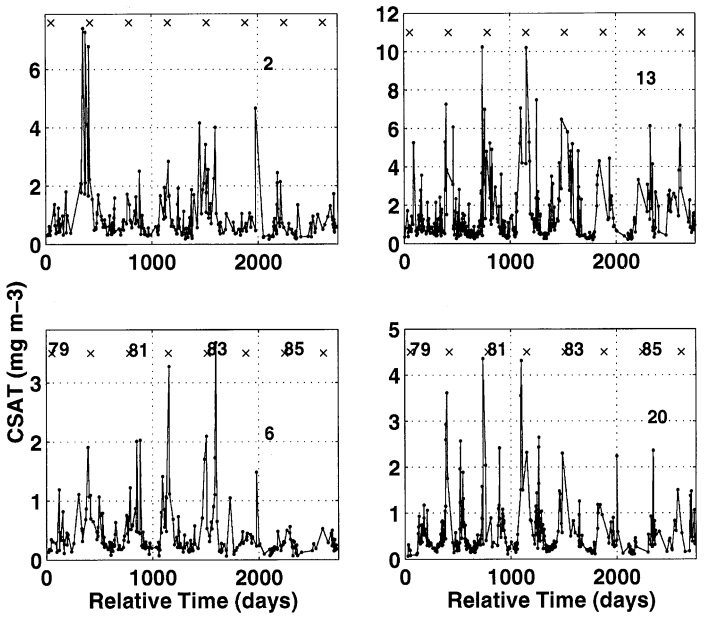

Fig. 8. Representative CSAT time series from SEA study areas 2 and 6 (leftmost panels) and NEA study areas 13 and 20 (rightmost panels) where the first and last days of the time series are 6 November, 1978, and 13 May, 1986, respectively. Note *y*-axis scale is different for each panel. As a reference, the first day of each calendar year is indicated by a small "×" with the year indicated in the lower panels.

Table 2
Multiple linear correlation coefficients from five sets of regressions between CSAT time series: (1) 8, NEA study areas representing middle shelf, outer shelf and slope waters; (2) SEA middle and outer shelf study areas; and (3) NEA; (4) SEA and (5) "Around Hatteras" along-shelf study areas. Number of observations for each regression is given in parentheses

NEA study areas ($n=169$)

	Middle			Outer			Slope	
	13	14	15	17	18	19	20	21
13	1.00	0.85	0.74	0.87	0.80	0.70	0.68	0.62
14	0.85	1.00	0.86	0.77	0.89	0.78	0.62	0.63
15	0.74	0.86	1.00	0.72	0.83	0.87	0.62	0.61
17	0.87	0.77	0.72	1.00	0.89	0.80	0.88	0.80
18	0.80	0.89	0.83	0.89	1.00	0.90	0.79	0.82
19	0.70	0.78	0.87	0.80	0.90	1.00	0.77	0.80
20	0.68	0.62	0.62	0.88	0.79	0.77	1.00	0.91
21	0.62	0.63	0.61	0.80	0.82	0.80	0.91	1.00

SEA study areas ($n=75$)

	Middle			Outer		
	2	3	4	6	7	8
2	1.00	0.82	0.66	0.87	0.80	0.60
3	0.82	1.00	0.75	0.74	0.83	0.69
4	0.66	0.75	1.00	0.74	0.81	0.90
6	0.87	0.74	0.74	1.00	0.91	0.78
7	0.80	0.83	0.81	0.91	1.00	0.86
8	0.60	0.69	0.90	0.78	0.86	1.00

NEA along-shelf ($n=130$)

	13	14	15	16	17	18	19
13	1.00	0.78	0.65	0.51	0.85	0.71	0.58
14	0.78	1.00	0.83	0.55	0.73	0.87	0.75
15	0.65	0.83	1.00	0.68	0.69	0.82	0.87
16	0.51	0.55	0.68	1.00	0.51	0.52	0.59
17	0.85	0.73	0.69	0.51	1.00	0.85	0.74
18	0.71	0.87	0.82	0.53	0.85	1.00	0.89
19	0.58	0.75	0.86	0.59	0.74	0.89	1.00

Around Cape Hatters ($n=82$)

	7	8	11	12
7	1.00	0.84	0.40	0.41
8	0.84	1.00	0.50	0.55
11	0.40	0.50	1.00	0.89
12	0.41	0.55	0.89	1.00

SEA along-shelf ($n=50$)

	5	6	7	8
5	1.00	0.85	0.76	0.70
6	0.85	1.00	0.86	0.78
7	0.76	0.86	1.00	0.85
8	0.70	0.78	0.85	1.00

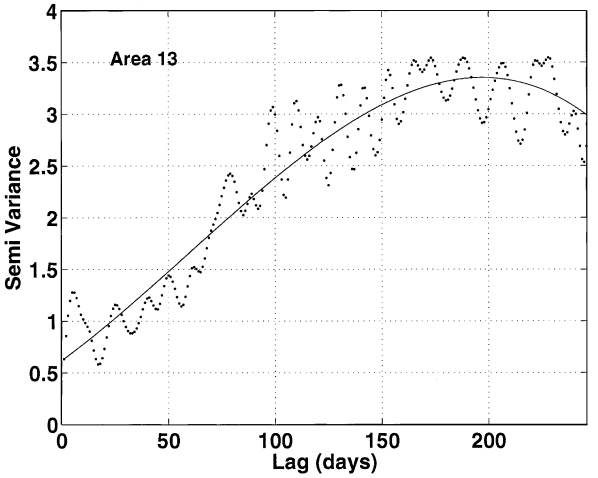

Fig. 9. Structure function (semi-variogram) for the CSAT time series from study area 13 (see Fig. 8). For the results shown in Table 3, SV0 is the value of the polynomial function fit to the data at lag = 1 day and SV1 is the value at the first major peak (lag = 195 days in this example), defined here as the point at which the slope of the polynomial fit to the data is equal to 0.

time series from all NEA and SEA shelf/slope study areas. Table 2 shows that patterns in adjacent study areas in both the along- and across-shelf direction are generally very well correlated ($r > 0.8$), although the Georges Bank time series (study area 16) is not well correlated ($r < 0.6$) with any of the other NEA study areas. The results from the three along-shelf comparisons illustrate how the correlation between time series decreases with separation distance between the study areas. For example, the results of the "Along Cape Hatteras" group show that time series from study areas south of Cape Hatteras (7, 8) are not as well correlated ($r = 0.5$ or less) with those north of Cape Hatteras (11, 12), as with time series from study areas within their respective regions (NEA or SEA).

We used structure functions (e.g. Yoder et al., 1987) to characterize dominant scales in each of the time series and to compare the relative magnitude of seasonal with day-to-day variability. As an example, Fig. 9 is a structure function or semi-variogram (plot of semi-variance (SV) versus time lag for lags up to 250 days apart) for the time series from study area 13 (see Fig. 8). In general, the structure functions were quite noisy as evidenced by the high SV at lag 1 and by the high variability at all lags around the trend evident in the polynomial fit to the data (see Methods). Using the polynomial curve fit to each of the semi-variograms, we calculated the lag time and SV associated with the first peak or asymptote, as well as the SV associated with the 1-day lag (Table 3). The time lag associated with the first peak or asymptote is half the period of the first dominant scale in the time series (e.g. Yost et al., 1982; Yoder et al., 1987). The results in Table 3 show that the mean half-period for the dominant scale (SV1) from shelf and slope water study areas of the SEA and NEA is 173 (S.D. = 46) and 184 (S.D. = 15) days, respectively, both of which are close (i.e. within one standard deviation) to 0.5 years (183 days). This analysis illustrates the overall dominance (along with considerable noise) of a simple seasonal pattern, i.e. a pattern described by a single biomass peak and minimum during the year. The SV1/SV0 ratio is an index indicating the relative magnitudes of the variability associated with the seasonal peak (SV1) versus

Table 3
Summary of the structure function results. SV0 and SV1 refer to semi-variance at the first time lag and at the first peak, respectively

Study area	Time (days) of Peak 1	SV1/SV0
1	175	3.9
2	250	4.2
3	120	1.7
4	160	2.1
5	180	4.3
6	223	7.0
7	118	1.7
8	154	3.9
SEA areas 1–8	173 (46)	3.6 (1.8)
9	189	9.3
10	100	10.1
11	178	5.7
12	205	7.1
13	195	3.4
14	185	2.9
15	181	2.9
16	190	3.6
17	200	4.3
18	169	5.0
19	200	4.4
20	158	4.3
21	170	3.4
NEA areas 11–21	184 (15)	4.3 (1.3)
All study areas	176 (35)	4.5 (2.2)

that associated with lag 1 (SV0), i.e. daily variability. The results show that for both the SEA and NEA shelf and slope water study areas (i.e. all except for study areas 9 and 10), the day-to-day variability (SV0) is very high in that the seasonal variability (SV1) is only about 4X greater on average. Of the 21 study areas, the Gulf Stream and "offshore" study areas (areas 9 and 10, respectively) have the lowest SV0 and SV1 values of all study areas. SV1/SV0 ratios (Table 3) and thus comparatively low daily variability in comparison to the shelf and slope water study areas.

3.4. Analyses of 45-day binned data

As illustrated by Fig. 10, time series of binned data (45-day bins) captured patterns at seasonal and longer time scales but as for all binned data, lost the higher frequency variability (compare Figs. 8 and 10). Fig. 11 shows both the daily and binned time series from study area 10 (located

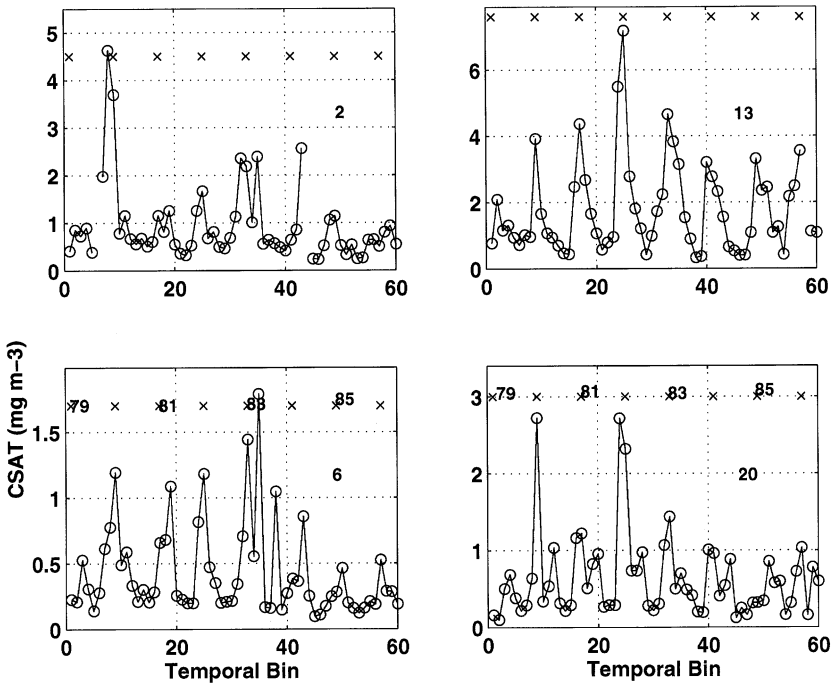

Fig. 10. CSAT time series of 45-day binned data from study areas 2, 6, 13 and 20 (compare with Fig. 8). Note y-axis scale changes between panels. As a reference, the first bin of each year is indicated by a small "×" with the year indicated in the lower panel.

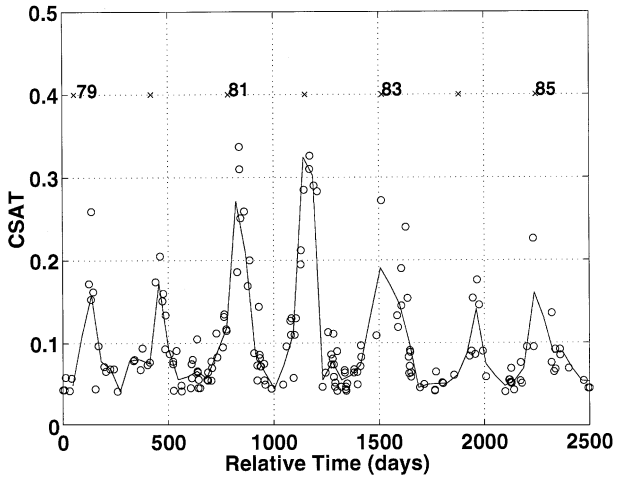

Fig. 11. CSAT time series of daily (circles) and 45-day binned data from study area 10 located in open ocean waters off the southeast US (see Fig. 2). As a reference, the first day of each calendar year is indicated by a small "×".

offshore of the Gulf Stream front, Fig. 2). Results from this study area were examined for evidence of long period trends or drift in CSAT concentrations, possibly indicative of poor quality CZCS data after August, 1981 (Evans and Gordon, 1994). However, Fig. 10 shows no apparent long-term trend in either the daily or binned CSAT values. For example, note that the annual minimum CSAT concentration is consistently near $0.05\,mg\,m^{-3}$. Simple statistics and regressions of CSAT versus relative time also indicated no long-term trend. Mean CSAT concentration of the first and last halves of the record were not significantly different: 0.11 (S.D. = 0.08, $n = 30$) and 0.09 (S.D. = 0.04, $n = 29$) $mg\,m^{-3}$, respectively, indicating a stationary time series (but with obvious periodic oscillations).

The time series of binned data from all 21 study areas showed markedly similar patterns which we confirmed using multiple linear regression. Using three separate multiple regressions (for SEA, NEA and all shelf regions), median r values were 0.71, 0.79 and 0.67, respectively. None of the series were negatively correlated with another, and correlations did not improve using time lags. This indicates that major seasonal features in the 45-day binned data time series are generally in phase.

Table 4 shows temporal (modes 1 and 2) and spatial (modes 1–4) EOF matrices as computed separately for SEA and NEA study areas. The corresponding amplitude time series are shown in

Table 4
Temporally and spatially normalized EOF matrices (and in parentheses, percent variability explained) for SEA and NEA study areas: modes 1 and 2 for temporal EOFs and modes 1–4 for spatial. Postive values are in bold

Temporal EOF matrix			Spatial EOF matrix			
Study area	Mode # (%)		Mode # (%)			
	1 (73)	2 (11)	1 (41)	2 (25)	3 (14)	4 (9)
1	**1.19**	−1.46	**1.67**	**0.88**	−0.77	**0.31**
2	**1.08**	−0.83	**0.33**	−1.81	**1.30**	**1.35**
3	**0.65**	**0.80**	−2.07	−0.34	−1.05	**0.03**
4	**0.89**	**1.16**	−0.61	**1.64**	**1.23**	**0.44**
5	**0.87**	−.73	**0.37**	−0.37	−1.72	**0.82**
6	**1.18**	−0.41	**0.49**	−0.85	**0.21**	−2.18
7	**1.03**	**0.85**	−0.18	**0.06**	**0.16**	−0.69
8	**1.00**	**1.33**	0.00	**0.55**	**0.34**	−0.10
	1 (78)	2 (8)	1 (51)	2 (19)	3 (14)	4 (18)
11	**1.03**	**0.97**	**1.05**	−0.44	−0.61	**0.05**
12	**1.14**	**0.73**	**0.45**	−0.46	**2.41**	−0.21
13	**1.02**	−0.32	**0.02**	−0.81	**0.21**	**0.98**
14	**0.97**	−1.21	−0.82	−0.57	−0.15	2.38
15	**0.93**	−1.92	−2.22	−1.26	−0.90	−1.41
16	**0.60**	−0.33	−1.12	**2.69**	−0.10	**0.44**
17	**1.04**	**0.90**	**0.48**	**0.52**	**0.17**	−0.15
18	**1.10**	−0.52	**0.47**	−0.52	−0.24	**0.37**
19	**1.10**	−0.76	−0.36	**0.30**	**1.32**	−1.17
20	**0.94**	**1.38**	**1.02**	**0.36**	−1.10	−0.47
21	**1.02**	**0.80**	**1.11**	**0.15**	−0.95	−0.63

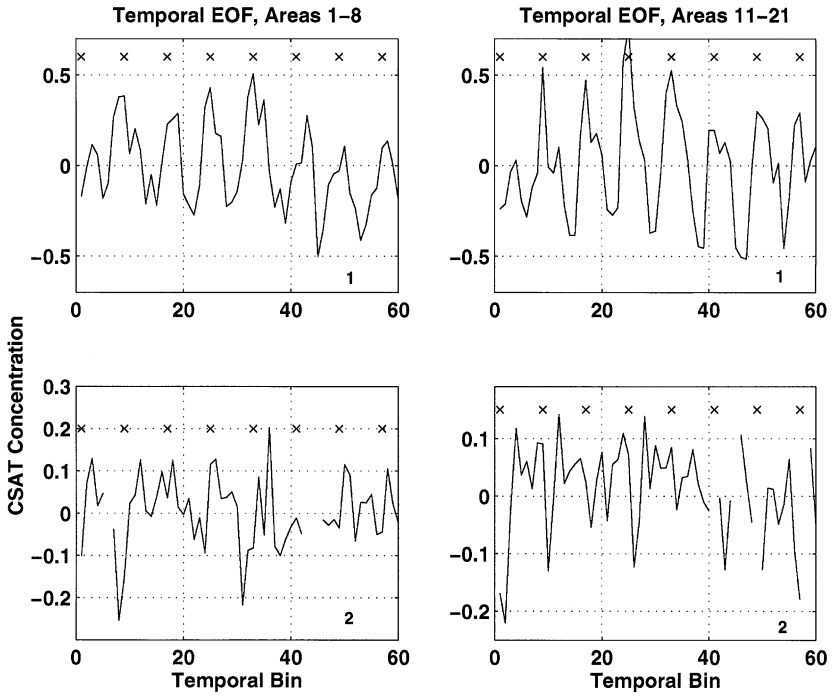

Fig. 12. EOF amplitude time series for modes 1 (upper panels) and 2 (lower panels) from temporally normalized EOF analyses for SEA shelf areas 1–8 (leftmost panels) and NEA study areas 11–21 (rightmost panels). Mode number is indicated in lower right, and the first day of each calendar year is indicated by a small "×". See Table 4 for EOF weighting factors.

Figs. 12 and 13. For both SEA and NEA study areas, the first 2 modes of the temporal EOFs are dominated by a simple seasonal pattern and accounted for 84% and 86% of the total variability in the binned data time series for areas 1–8 and 11–21, respectively. The dominance of the seasonal cycle in the 7.5-year CSAT time series is particularly evident in the first mode of the temporal EOFs, which accounted for 73% and 78% of the variability in the SEA and NEA, respectively. For the temporal EOFs, the second mode for areas 1–8 modifies the mean seasonal pattern in a complex way. The EOF values in Table 4 (i.e. positive values for areas 3, 4, 7 and 8) show that the mode 2 adjustments to the seasonal cycle in the northern study areas are generally out of phase with the southern study areas in the SEA. In the NEA, Mode 2 of the temporal EOFS is also associated with along-shelf variability and separates patterns in the outer shelf and slope study areas in the south (i.e. Table 4 shows positive EOF weighting values for mode 2 for study areas 11, 12, 17, 20 and 21) from other NEA middle shelf, outer shelf and slope waters. The effect of mode 2 on these 5 areas is for relatively lower (in comparison to the mean) concentrations in winter (i.e. positive weights in Table 4 and negative amplitudes in Fig. 12) and generally higher concentrations during other seasons.

Spatial EOFs emphasize temporal changes to the general mean spatial pattern, i.e. when one or more of the study areas changes disproportionately more (or less) with time than the others. In other words, spatial EOFs show little or no effects if the initial spatial relations (CSAT gradient)

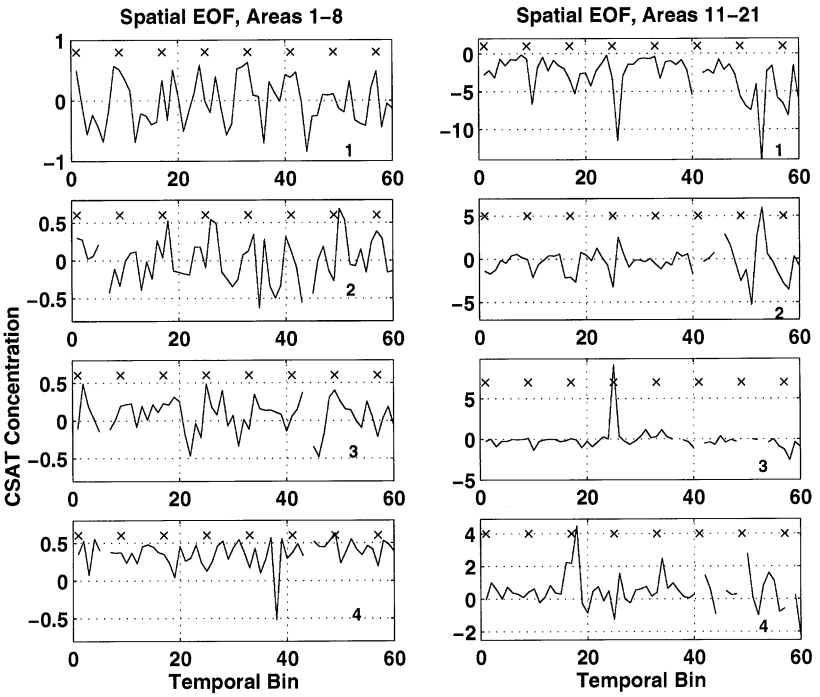

Fig. 13. EOF amplitude time series for modes 1–4 from spatially-normalized EOF analyses for SEA shelf areas 1–8 (leftmost panels) and NEA study areas 11–21 (rightmost panels). Mode number is indicated in lower right, and the first day of each calendar year is indicated by a small "×". See Table 4 for EOF weighting factors.

between the study areas are maintained throughout the time series. Table 4 shows that in the SEA, mode 1 (41% of the variability) of the spatial EOFs is associated with along-shelf variability in that the north Florida shelf study areas (positive EOF weighting factors for areas 1, 2, 5 and 6) have relatively high CSAT concentrations in winter and relatively low concentrations in summer in relation to the other 4, more northerly study areas. Mode 2 (25%) appears to be dominated by differences between areas 1, 4 and 8 (northern and southern extremes) versus the study areas in the central portion of the bight. Mode 4 (9%) is associated with across-shelf variability. An interesting result is that except for Mode 4, the first 4 SEA modes shows little effect of across-shelf variability, i.e. the across-shelf CSAT gradient, a prevalent feature in Fig. 3, is consistently maintained throughout the time series.

Spatial EOFs for NEA study areas yielded somewhat different results than for the SEA. As for the SEA, mode 1 for the NEA study areas (51% of the variability) was also related to along-shelf variability in that it separated CSAT patterns in the more northern shelf waters (study areas 14, 15, 16 and 19 with negative weighting factors, Table 4) from shelf and slope waters farther south (positive weighting factors in Table 4). Thus, the effect of mode 1 is for relatively high concentrations in the north (negative EOFs and negative amplitudes) compared to the more southerly study areas, particularly in the winter and spring. In the NEA, mode 2 (19%) was related to across-shelf variability, i.e. differences between middle shelf regions (areas 11–15) and outer shelf and slope waters (areas 17, 19, 20 and 21). In addition, Georges Bank (area 16) had a

uniquely high and positive EOF value (Table 4). The effect of mode 2 is complex, but one of the general effects is for relatively low CSAT concentrations in outer shelf and slope waters in the spring and summer compared to the middle shelf. Based on the amplitude time series (Fig. 13), NEA modes 3 (14%) and 4 (8%) were dominated by changes in the mean spatial patterns associated, respectively, with 1982/83 (temporal bin 25) and 1981/82 winter peaks (temporal bin 18). These were the only clear indications of interannual variability in the spatial relations among the time series.

For SEA and NEA study areas, the first 4 temporal EOF modes accounted for 93 and 94%, respectively, of the total variability in the 45-day binned time series. Fig. 14 shows examples of time series reconstructed from the first 4 EOF modes plotted with the original daily time series (from which the 45-day binned time series were derived). The reconstructed time series do a good job of reproducing seasonal and longer period structure, but clearly miss a considerable amount of the total variability present within the original daily time series. How much of the total variability in the original time series in associated with time scales of 1–45 days and thus averaged out of the binned time series? To answer this question, we regressed Log_{10}CSAT values from the each of the original 21 times series versus the appropriate 45-day mean value from the reconstructed time series. From these regressions, r^2 values ($\times 100$) for the SEA study areas ranged from 34% (for study area 3) to 66% (study areas 6 and 8) with an average of 53%; and for the NEA study areas, from only 21% (study area 16) to 66% (study areas 11, 12 and 20) with an

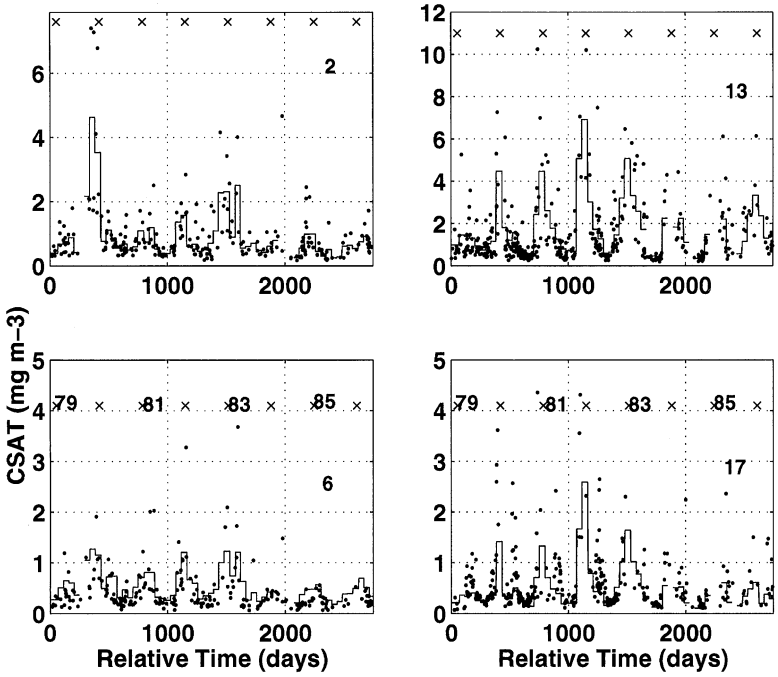

Fig. 14. Daily CSAT time series (small dots) and the time series reconstructed from modes 1–4 of the EOF analyses of the 45-day binned time series (solid line) for study areas 2, 6, 13 and 17. Note y-axis scale changes between panels. As a reference, the first day of each calendar year is indicated by a small "×" with the year indicated in the middle panel.

average of 55%. These results indicate that the higher frequency (ca. Time scales, less than 45 days) variability accounts for about 44% on average of the total variability in the original time series and ranges from 34% to 79%.

4. Discussion

4.1. Overview of results

Using 7.5 years of CZCS imagery we were able to quantify major time/space CSAT distribution patterns in ocean margin (continental shelf and slope) waters off the US East coast. In particular, we focused on patterns in mean CSAT concentration averaged over 21 study areas representing rather large ($>100\,km^2$) shelf/slope regions. We did not examine spatial variability within our 21 study areas, but previous studies of ocean margin waters, including one off the southeast US (Yoder et al., 1987) indicate that such variability will also be important (Smith et al., 1988, Denman and Abbott, 1988). Our CSAT observation interval was nominally one-day, but consecutive day sampling was not often realized owing to cloud cover, and because the CZCS sensor was switched off during many passes over the US coast. Some of our analyses required few or no missing observations, so we placed CSAT data into 45-day bins to build a continuous time series. With additional caveats discussed below, our results (for waters seaward of the 20-m isobath) show:

(1) a simple annual CSAT cycle common to all ocean margin waters along the entire US East Coast, consisting of a broad peak in CSAT concentration during winter and minimum concentrations during the summer;
(2) relatively subtle across- and along-shelf changes to the timing and relative magnitude of the winter CSAT maxima and summer minima, as well as the presence of secondary seasonal peaks in some regions (e.g. spring peak in outer shelf and slope waters of the NEA);
(3) high variability at time scales of days to weeks superimposed on the seasonal pattern;
(4) high spatial coherence of the seasonal component between all 21 study areas;
(5) high coherence of the days-to-weeks component between study areas near each other, but generally low coherence for study areas far apart; and
(6) detectable, but low interannual variability.

4.2. Comments on seasonal phytoplankton blooms

For 45-day binned data (i.e. variability at periods shorter than 45-days was averaged out), a simple conceptual model of relatively high CSAT concentrations during winter and relatively low concentrations during summer, with a smooth transition between the two periods, explains 67–78% of the variability of the 21 study areas based on the temporal EOFs. Regressions among the 21, 45-day binned time series (at zero lag) yielded high positive correlation coefficients demonstrating that this simple pattern is prevalent in CSAT imagery of shelf/slope waters all along the US East Coast. A previous study of CZCS imagery of continental shelf waters off North

Carolina (SABRE Study Area) showed a similar dominant, seasonal pattern (Barnard et al., 1997). Extensive in situ data observations within the NEA region during the same era as CZCS observations also show the same general seasonal pattern (O'Reilly and Zetlin, 1998, Table 3). Agreement with the in situ data is strong evidence that the CSAT patterns in our 21 study areas (all in waters offshore of the 20-m isobath) represent chlorophyll *a* patterns in these waters and are not caused by processing artifacts or by high concentrations of colored dissolved organic matter (CDOM).

This and other satellite studies (Yoder et al., 1993; Banse and English, 1994; Barnard et al., 1997; Fuentes-Yaco et al., 1997) present a somewhat different view of seasonal phytoplankton bloom dynamics than the conventional interpretation (e.g. Cushing, 1959), particularly regarding the winter-spring bloom at mid latitudes. The conventional view of a spring or fall phytoplankton biomass bloom is a rapid increase in biomass over a period of weeks in response to changing stratification and light conditions during winter/spring. Fall blooms are related to increases in nutrient concentrations owing to wind-induced de-stratification and vertical mixing. The period of rapid increase is then followed by a period of rapid decrease owing to nutrient limitation and grazing in the case of spring blooms or by light limitation in the case of fall blooms (e.g. Cushing, 1959).

In contrast, our results for ocean margin waters between Cape Canaveral and Cape Cod show two basic states: low and high CSAT concentrations (summer and winter, respectively) with a gradual change in state between the two extremes. The high CSAT season is not a "pulse" but rather a broad peak extending over many months. Furthermore, this basic pattern is coherent between waters of different depth ranges (but all >20-m depth), over almost 20° of latitude and between two different oceanographic regimes (SEA and NEA) having very different nutrient dynamics (e.g. Bishop et al., 1980; Yoder, 1985). Our observations suggest a common mechanism but not the traditional Sverdrup (1953) model for seasonal blooms, in which phytoplankton biomass increases with seasonal increases in the mean irradiance level of the mixed layer. Some of the high frequency (i.e. <45 day time scales) variability we observed may be related to transient pulses in biomass that may occur prior to stratification (e.g. Townsend et al., 1994).

The seasonal CSAT pattern we observe is similar to Longhurst's Model 3 (Longhurst, 1995, 1998), "Winter–Spring Production with Nutrient Limitation". According to Longhurst (1995), this model applies primarily to offshore waters at mid-latitudes (which includes almost half the area of the global ocean). The main characteristics (Longhurst, 1995) are: (1) productivity is not limited by light and increases during winter owing to increased nutrient supply; (2) nutrient-limitation occurs during summer, (3) and phytoplankton biomass accumulates in winter but not during spring, although primary production is higher in spring. The latter is consistent with relatively close coupling between phytoplankton growth and zooplankton consumption (Banse and English, 1994). Productivity is generally relatively low in the open ocean waters with Model 3 behavior (Longhurst, 1995), but that is clearly not the case for the NEA and SEA (e.g. Falkowski et al., 1983; Yoder et al., 1985). This simple model probably does not apply to all shelf and slope locations off the US East Coast (and note that we excluded all waters shoaler than 20-m from any of our analyses) and perhaps is limited to near-surface waters only. As our CSAT observations are consistent with the general pattern predicted from Longhurst's Model 3 (Longhurst, 1995), seasonal changes in solar irradiance as a direct regulator of seasonal phytoplankton growth may not be as important in middle shelf to slope waters of the NEA

as previously believed. However, the effect of seasonal changes in solar irradiance on seasonal changes to vertical density stratification is important. Stratification, and subsequent nutrient limitation of the mixed layer, is the cause of low CSAT concentrations during summer compared to winter.

Secondary spring CSAT peaks in NEA slope waters (e.g. study areas 20 and 21) are an important exception to the simple seasonal pattern discussed above. Such peaks were also observed in the MARMAP chlorophyll *a* data (O'Reilly and Zetlin, 1998), in other satellite studies (Brown et al., 1985; Garcia-Moliner and Yoder, 1994) and to some extent, in the chlorophyll fluorescence record from a fluorometer moored for 15 months at 20-m depth near the 80-m isobath in the southern Mid Atlantic Bight (NEA) (Flagg et al., 1994). A previous study of temporal/spatial patterns in CZCS imagery from the NEA region (Eslinger et al., 1989) showed a shelf-wide April bloom, but this study only used imagery from 28 February to 9 July, 1979. By missing the winter period, the conclusions thus apply only to the relative change that occurs between spring and summer, and thus do not preclude a broad winter peak. An interesting difference between our CSAT results (as well as the near-surface MARMAP chlorophyll *a* data) and the fluorometer record (Flagg et al., 1994) is that the latter shows relatively high chlorophyll *a* concentrations during summer compared to winter. This difference may reflect subsurface chlorophyll *a* maximum layers detected by the 20-m moored fluorometer but not by CSAT. For example, MARMAP results show that chlorophyll *a* concentration is higher at 20-m depth than at the surface in outer shelf waters of the Southern MAB (which encompasses the location of the fluorometer mooring) from April through September (see Fig. 23 in O'Reilly and Zetlin, 1998). In productive shelf and slope waters (i.e. with K_{490} greater than ca. $0.10\,m^{-1}$), satellite ocean color scanners cannot detect the contribution to water-leaving radiance of chlorophyll *a* below about 10-m depth. Thus, our CSAT observations are observing a different part of the water column than did the moored fluorometer, and the results cannot be directly compared during the stratified seasons of the year.

4.3. Variability at time scales from days to weeks

Our index (from structure functions) comparing day-to-day variability with seasonal (i.e. 180-day periods) showed that the former averaged 25% of the latter. Furthermore, our regression analyses (i.e. between the original daily time series and EOF-reconstructions of the 45-day binned time series) show that variations at time scales ranging from 1–45 days accounted for an average of 44% of the total CSAT variability in the original 21 time series. These results indicate that the mean seasonal pattern is only part of the temporal "story" of the 21 study areas, as is obvious from the plots of the original CSAT time series. It is not surprising that such a high percentage of the CSAT variability occurs at days to week time scales, as "event" time scale phenomena are well documented in East Coast margin waters (e.g. Walsh et al., 1978; Yoder et al., 1981). Our results show that a major difference between event and seasonal CSAT variability is that the former decorrelates rapidly with separation distance of the study areas, whereas the mean seasonal cycle is highly correlated among all of the study areas. Spatial decorrelation at the event time scale is entirely consistent with local-scale forcing of events, such as upwelling and storm-induced mixing, plumes, frontal dynamics, etc. (Denman and Abbott, 1988).

4.4. Implications for using composite images to represent a mean annual cycle

Chlorophyll *a* concentrations from ocean color images are now a primary source of data for initializing and validating numerical models and for regional to global-scale calculations of ocean primary production (e.g. Platt and Sathyendranth, 1988). As clouds frequently obscure significant parts of daily ocean color images, investigators generally "composite" multiple images (i.e. pixel-by-pixel average where possible or select a single valid pixel to represent the temporal average where only one value is available) at weekly to monthly time scales to increase spatial coverage of their study domain. Our results show that 45-day composites will capture on average approximately half (56%) of the temporal variability in CSAT concentration in the 1 to 45-day window for ocean margin waters seaward of the 20-m isobath in our NEA and SEA study areas. Approximately half (44%) of the variability in this temporal domain will not be reflected in 45-day composites (and in fact, an undetermined fraction of the latter is probably noise, so that 45-day composites may capture more than 56% of the signal). Using this and other information from our study, one can envision the following or similar scenario for parameterizing NEA and SEA CSAT variability within regional to basin-scale models or calculations. A spatially coherent pattern with ca. 45-day resolution represents the mean annual cycle with peak magnitudes dependent on location (study area). This mean seasonal pattern is then modified by adding a "high" frequency component using an appropriate ratio of "high" to "low" frequency variability to determine high frequency peak magnitudes. In contrast to the mean seasonal cycle, the latter component should also include a decorrelation length-scale (which was not determined on our study).

4.5. Interannual variability

The general annual pattern was remarkably persistent throughout the 7.5 year record as evidenced by the EOF analyses, as well as visible inspection of the time series. For example, we did not see the rather larger interannual signals observed in CSAT imagery in ocean margin waters off the US west coast (Thomas and Strub 1990), presumably because ocean margin waters off the US east coast are not affected by strong, interannual climate signals such as *ENSO*. However, some of the EOF modes, as well as the time series graphs, indicated that CSAT patterns in winter, 1981/82 and 1982/83 were different in the NEA than other years. In general, CSAT concentrations in the NEA were higher during these two winters than in other years. The timing of this anomaly coincides with a change in the North Atlantic Oscillation (NAO) index from negative to positive. This transition is associated with anomalous southerly flow over the eastern United States and high river runoff (Hurrell, 1995; Guetter and Georgakakos, 1993). As one can easily develop arguments relating enhanced CSAT concentrations to increased upwelling (southerly flow), stratification or nutrient input (both potentially associated with river runoff), an NAO related explanation for these anomalies is tempting. However, the index continued to be high during the remaining years of the 1980s (Hurrell, 1995), and positive river runoff anomalies peaked in 1984 and 1985 (Guetter and Georgakakos, 1993). In fact, salinity and temperature anomalies in the NEA from 1981 until mid 1983 were not unusual compared to high positive anomalies in 1980 and 1985 and generally negative anomalies during the latter part of 1983 and in 1984 (Mountain and Manning, 1994). Thus, changes to the NAO index and associated meteorological and

oceanographic conditions probably do not explain high CSAT concentration during winter of 1981/82 and 1982/83.

The CZCS sensor was a proof-of-concept mission with no formal calibration or validation program during the mission (Evans and Gordon, 1994). Nevertheless, the results were used for many studies of temporal and spatial variability, although usually with caveats regarding the absolute values of the concentrations (McClain et al., 1998). Our study focused only on the data from one satellite sensor, but imagery from new sensors (e.g. OCTS, Sea WiFS) are now available and more are planned over the next decade (IOCCG 1998). The potential exists to use imagery from multiple sensors to determine long term trends in ocean margin waters going back in some cases to the CZCS era. To realize this potential, however, will require considerable effort to understand how different sensor specifications, bio-optical algorithms and other characteristics affect multi-sensor time series. This a difficult challenge, and we are involved with continuing efforts to improve the accuracy of CZCS data and to relate its imagery to those acquired from the new generation of ocean color sensors.

Acknowledgements

We thank NASA's Earth Science Enterprise Office and the University of Rhode Island for financial support; Drs. G. Feldman, C. McClain, the DAAC and others at Goddard Space Flight Center for their efforts to develop satellite ocean color products and to efficiently distribute the imagery; and S.E. Schollaert for assistance with the color figures.

References

Banse, K., English, D.C., 1994. Seasonality of coastal zone color scanner phytoplankton pigment in the offshore oceans. Journal of Geophysical Research 99, 7323–7345.

Barnard, A.H., Stegmann, P.M., Yoder, J.A., 1997. Seasonal surface ocean variability in the South Atlantic Bight derived from CZCS and AVHRR imagery. Continental Shelf Research 17, 1181–1206.

Beardsley, R.C., Boicourt, W.C., Hansen, D.V., 1976. Physical oceanography of the Middle Atlantic Bight. In: Gross, M.G. (Ed.), Middle Atlantic Continental Shelf and the New York Bight Limnology and Oceanography Special Symposia, Vol. 2. American Society of Limnology and Oceanography, Inc.

Bisagni, J.J., O'Reilly, J.E., Barnard, A.H., Wolfteich, C.M., 1997. Determination of optimum aerosol optical thickness ratios for atmospheric correction of coastal zone color scanner data in the Georges Bank—Gulf of Maine Region. Continental Shelf Research 17, 635–654.

Bishop, S.S., Yoder, J.A., Paffenhofer, G.-A., 1980. Phytoplankton and nutrient variability along a cross-shelf transect off Savannah, Georgia, USA. Estuarine, Coastal, and Marine Science 11, 359–368.

Brown, O.B., Evan, R.H., Brown, J.W., Gordon, H.R., Smith, R.C., Baker, K.S., 1985. Phytoplankton blooming off the US East Coast: A satellite description. Science 229, 163–167.

Clark, D.K., 1981. Phytoplankton pigment algorithms for the Nimbus-7 CZCS. In: Gower, J.F.R. (Ed.), Oceanography from Space. Plenum Press, New York, pp. 227–237.

Csanady, G.T., 1990. Physical basis of coastal productivity. Eos 71, 1060–1065.

Cornillon, P., 1992. Gulf Stream. In: Encyclopedia of Earth System Science, Vol. 2. Academic Press, New York, pp. 465–480.

Cushing, D.H., 1959. The seasonal variation in oceanic production as a problem in population dynamics. J. Cons. Int. Explor. Mer. 24, 455–464.

Denman, K.L., Abbott, M.R., 1988. Time evolution of surface chlorophyll patterns from cross-spectrum analysis of satellite color. Journal of Geophysical Research 93, 6789–6998.

Eslinger, D.L., O'Brien, J.J., Iverson, R.L., 1989. Empirical orthogonal function analysis of cloud-containing Coastal Zone Color Scanner images of northeastern North American coastal waters. Journal of Geophysical Research 94, 10 884–10 890.

Evans, R.H., Gordon, H.R., 1994. Coastal zone color scanner "system calibration": a retrospective examination. Journal of Geophysical Research 99, 7293–7307.

Falkowski, P.G., Vidal, J., Hopkins, T.S., Rowe, G.T., Whitledge, T.E., Harrison, W.G., 1983. Summer nutrient dynamics in the Middle Atlantic Bight: primary productivity and the utilization of phytoplankton carbon. Journal of Plankton Research 5, 515–537.

Feldman, G., Kuring, N., Ng, C., Esaias, W., McClain, C., Elord, J., Maynard, N., Endres, D., Evans, R., Brown, J., Walsh, S., Carle, M., Podesta, G., 1989. Ocean color: the availability of the global data set. Eos 70 (23), 634.

Flagg, C.N., Wirick, C.D., Smith, S.L., 1994. The interaction of phytoplankton, zooplankton and currents from 15 months of continuous data in the Mid-Atlantic Bight. Deep-Sea Research II 41, 411–436.

Fuentes-Yaco, C., Vezina, A.F., Larouche, P., Vigneau, C., Gratton, Y., Gosselin, M., 1997. Phytoplankton pigment in the Guld of St. Lawrence, Canada, as determined by the Coastal Zone Color Scanner— Part II: multivariate analysis. Continental Shelf Research 17, 1441–1459.

Garcia-Moliner, G., Yoder, J.A., 1994. Variability in pigment concentration in warm-core rings as determined by coastal zone color scanner satellite imagery from the Mid-Atlantic Bight. Journal of Geophysical Research 99, 14 277–14 290.

Gordon, H.R., Clark, D.K., Brown, J.W., Brown, O.B., Evans, R.H., Broenkow, W.W., 1983. Phytoplankton pigment concentrations in the Middle Atlantic Bight: comparison of ship determinations and CZCS estimates. Applied Optics 22, 20–36.

Guetter, A.K., Georgakakos, K.P., 1993. River outflow of the conterminous United States, 1939–1988. Bulletin of the American Meteorological Society 74, 1873–1891.

Hurrell, J.W., 1995. Decadal trends in the North Atlantic Oscillation: Regional temperatures and precipitation. Science 269, 676–679.

Lee, T.N., Yoder, J.A., Atkinson, L.P., 1991. Gulf Stream frontal eddy influence on productivity of the southeast US continental shelf. Journal of Geophysical Research 96, 22 191–22 205.

Longhurst, A., 1995. Seasonal cycles of pelagic production and consumption. Progress in Oceanography 36, 77–167.

Longhurst, A., 1998. Ecological Geography of the Sea. Academic Press, New York, 398 pp.

Marra, J., Houghton, R.W., Garside, C., 1990. Phytoplankton growth at the shelf-break front in the Middle Atlantic Bight. Journal of Marine Research 48, 851–868.

McClain, C.R., Yoder, J.A., Atkinson, L.P., Blanton, J.O., Lee, T.N., Singer, J.J., Muller-Karger, F., 1988. Variability of surface pigment concentrations in the South Atlantic Bight. Journal of Geophysical Research 93, 10 675–10 697.

McClain, C.R., Cleave, M.L., Feldman, G.C., Gregg, W.W., Hooker, S.B., Kuring, N., 1998. Science quality Sea WiFS data for global biosphere research. Sea Technology 39, 10–16.

Menzel, D.W., Pomeroy, L.R., Lee, T.N., Blanton, J.O., Alexander, C.R., 1993. Introduction. Ocean Processes: US Southeast Continental Shelf. National Technical Information Service, Springfield, VA, DE93010744, 112 pp.

Mountain, D.G., Manning, J.P., 1994. Seasonal and interannual variability i the properties of the surface waters of the Gulf of Marine. Continental Shelf Research 14, 1555–1581.

O'Reilly, J.E., Zetlin, C., 1998. Seasonal, horizontal, and vertical distribution of phytoplankton chlorophyll *a* in the northeast US continental shelf ecosystem. NOAA Technical Report NMFS 139, US Department of Commerce, Seattle.

Platt, T., Sathyendranath, S., 1988. Oceanic primary production: estimation by remote sensing at local and regional scales. Science 241, 1613–1619.

Pribble, J.R., Walsh, J.J., Dieterle, D.A., 1994. A numerical analysis of shipboard and coastal zone color scanner time series of new production within Gulf Stream cyclonic eddies in the South Atlantic Bight. Journal of Geophysical Research 99, 7513–7538.

Riley, G.A., 1946. Factors controlling phytoplankton populations on Georges Bank. Journal of Marine Research 6, 54–73.

Riley, G.A., 1947. Seasonal fluctuations of the phytoplankton population in New England coastal waters. Journal of Marine Research 6, 114–125.

Ryan, J.P., Yoder, J.A., 1996. Long-term mean and event-related pigment distributions during the unstratified period in South Atlantic Bight outer margin and middle shelf waters. Continental Shelf Research 16, 1165–1183.

Ryan, J.P., Yoder, J.A., Cornillon, P.C., 1999a. Enhanced chlorophyll at the shelfbreak of the Mid-Atlantic Bight and Georges Bank during the spring transition. Limnology and Oceanography 44, 1–11.

Ryan, J.P., Yoder, J.A., Barth, J.A., Cornillon, P.C., 1999b. Chlorophyll enhancement and mixing associated with meanders of the shelf break front in the Mid-Atlantic Bight. Journal of Geophysical Research 104, 23 479–23 493.

Ryther, J.H., Yentsch, C.S., 1958. Primary production of continental shelf waters off New York. Limnology and Oceanography 3, 327–335.

Smith, R.C., Zhang, X., Michaelsen, J., 1988. Variability of pigment biomass in the California Current system as determined by satellite imagery. 1. Spatial variability. 1988. Journal of Geophysical Research 93, 10 863–10 882.

Sverdrup, H.U., 1953. On conditions for the vernal blooming of phytoplankton, J. Cons. Perm. Int. Exp. Mer. 18, 287–295.

Thomas, A.C., Strub, P.T., 1990. Seasonal and interannual variability of pigment concentrations across a California Current frontal zone. Journal of Geophysical Reseach 95, 13 023–13 042.

Townsend, D.W., Cammen, L.M., Holligan, P.M., Campbell, D.E., Pettigrew, N.R., 1994. Causes and consequences of variability in the timing of spring phytoplankton blooms. Deep-Sea Research 41, 747–765.

Verity, P.G., Lee, T.N., Yoder, J.A., Paffenhofer, G.-A., Blanton, J.O., Alexander, C.R., 1993. Processes on the outer continental shelf. Ocean Processes: US Southeast Continental Shelf, National Technical Information Service, Springfield, VA, DE93010744, 112 pp.

Walsh, J.J., Whitledge, T.E., Barvenik, F.W., Wirick, C.D., Howe, S.O., Esaias, W.E., Scott, J.T., 1978. Wind events and food chain dynamics within the New York Bight. Limnology and Ocanography 23, 659–683.

Walsh, J.J., Dieterle, D.A., Esaias, E.E., 1987. Satellite detection of phytoplankton export from the mid-Atlantic bight during the 1979 spring bloom. Deep-Sea Research 34, 675–703.

Yoder, J.A., 1985. Environmental control of phytoplankton production on the southeastern US continental shelf. In: Atkinson, L.P., Menzel, D.W., Bush, K.A. (Eds.), Oceanography of the Southeastern US Continental Shelf. AGU Press, Washington, DC, pp. 93–103.

Yoder, J.A., Atkinson, L.P., Lee, T.N., Kim, H.H., McClain, C.R., 1981. Role of Gulf Stream frontal eddies in forming phytoplankton patches on the outer southeastern shelf. Limnology and Oceanography 26, 1103–1110.

Yoder, J.A., McClain, C.R., Blanton, J.O., Oey, L.Y., 1987. Spatial scales in CZCS-chlorophyll imagery of the southeastern US continental shelf. Limnolgy and Oceanography 32, 929–941.

Yoder, J.A., McClain, C.R., Feldman, G.C., Esaias, W.E., 1993. Annual cycles of phytoplankton chlorophyll concentrations in the global ocean: A satellite view. Global Biogeochemical Cycles 7, 181–194.

Yost, R.S., Uehara, G., Fox, R.L., 1982. Geostatistical analysis of soil chemical properties of large land areas. 1. Semi-variograms. Soil Science Society of America Journal 46, 1028–1037.